

ACOUSTIC PYROMETRY FOR FLOW VELOCITY ESTIMATION: PRELIMINARY ANALYSIS

Gianluca Caposciutti, Lorenzo Ferrari

University of Pisa (DESTeC)

Largo Lucio Lazzarino, 1

56122 – Pisa – Italy

lorenzo.ferrari@unipi.it

ABSTRACT

Acoustic pyrometry uses the variations of the speed of sound in a medium to determine its temperature. One of the assumptions at the base of this technique is that the flow velocity component in the direction of the acoustic path is negligible in comparison to the speed of sound. However, if the temperature of the medium is known, the acoustic pyrometry approach can be used to determine flow speed, as long as the flow is not perpendicular to the acoustic path. The combined approach of temperature and velocity determination is also known as acoustic tomography. This technique allows the determination of velocity and temperature maps in a flow region. Even though this is an interesting result, the mathematical approach to solve the velocity and temperature fields might be very complex and sensitive measurement set-up. In this study, a preliminary investigation is carried out to determine the flow velocity by starting from the time of flight of an acoustic signal moving along different acoustic paths in a constant temperature field. For this purpose, a simplified geometry is considered. The developed mathematical approach at the base of the methodology is presented in this study.

INTRODUCTION

Recently an increasing interest is being paid to acoustic pyrometry as it allows the estimation of a temperature distribution in a section with virtually no interactions with the flow. Acoustic pyrometry is based on the measurement of the time of flight of an acoustic wave along a known path. As the propagation speed of the wave is directly related to medium temperature, the travelling time of the wave can be related to the encountered temperature. If the temperature is not uniform, multiple emitter-receiver couples (ERCs) laying on the same plane can be used to reconstruct a temperature map in a section. These measurements are generally performed in a section perpendicular to flow velocity. In this way (under the hypothesis of a subsonic flow) the impact of flow velocity on

temperature estimation may be considered as negligible. On the other hand, the flow velocity component along the acoustic path may be estimated with a similar approach if the flow temperature is known and an acoustic path which is not perpendicular to flow velocity vector is considered. In this case, the time-of-flight measurement provides an apparent sound speed that can be used to estimate the flow velocity component along the acoustic direction.

By combining both approaches, typically by considering two adjacent sections instrumented with several ERCs, is it possible to estimate in a region both the flow velocity and the temperature maps. In this case, the technique is named: acoustic tomography [1,2]. In a first analysis step, the temperature map in the two sections and in the region in between is estimated directly and by interpolation, respectively. In a second analysis step, once the temperature distribution is supposed as known, the velocity field may be reconstructed by considering the ERCs in the two opposite sections. As velocity and temperature are generally not uniform, a complex mathematical approach is necessary to determine the two maps. Being a first approach to acoustic tomography, in this study the problem has been simplified to specifically focus on the problem of estimating a flow velocity map by considering the time-of-flight of an acoustic wave.

METHOD

This study aims at investigating the potential capability of an acoustic pyrometry setup for the estimation of flow velocity. To this purpose, a circular duct with a diameter of 1 meter was considered as a case study. By using a set of coplanar microphones/emitter couples (ERCs), the time-of-flight τ of an acoustic wave travelling at the speed of sound c through the medium between them was measured, and the velocity profile inside the duct on the ERCs plane Ω was reconstructed. In particular, the time-of-flight of the acoustic wave is influenced by the speed of sound, by the distance l between the emitter and the receiver of a ERC, and

by the fluid local speed U and its angle α with the connecting line connecting the emitter receiver couple. A scheme is showed in Fig.1.

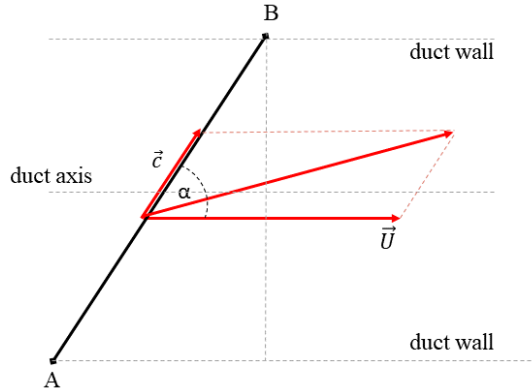


Figure 1. Relationship between the acoustic wave travelling speed and the fluid speed.

To reduce the problem complexity, sound paths were considered as straight lines between the receiver and the emitter, and any distortion effects that may be caused by the flow speed or the interactions with the domain walls were neglected. Therefore, the speed of sound is affected by U so as:

$$\tau_{AB} = \int_A^B \frac{1}{c + U \cos(\alpha)} dl \quad (1)$$

In Eq.1, it is intended that the integral is calculated along the A→B path. According to [3], emitter and the receiver may be switched, thus the time of flight can be described as:

$$\tau_{BA} = \int_B^A \frac{1}{c - U \cos(\alpha)} dl = - \int_A^B \frac{1}{c - U \cos(\alpha)} dl \quad (2)$$

By subtracting Eq.2 to Eq.1, the difference in time-of-flight, $\Delta\tau$, is obtained as:

$$\Delta\tau = \int_A^B \frac{c + U \cos(\alpha) - c + U \cos(\alpha)}{(c^2 - U^2 \cos^2(\alpha))} dl \Rightarrow \quad (3)$$

$$\Delta\tau = \int_A^B \frac{2U \cos(\alpha)}{(c^2 - U^2 \cos^2(\alpha))} dl$$

In this study, as subsonic conditions are considered ($c^2 \gg U^2$), hence $\Delta\tau$ may be wrote as:

$$\frac{\Delta\tau}{2} = \int_B^A \frac{U \cos(\alpha)}{c^2} dl \quad (4)$$

Eq.4 provides the non-linear relation between U , α and the measured difference in time of flight between two emitter-receiver couples. Under the hypothesis of considering an ideal gas, the speed of sound c can be calculated by the fluid physical characteristic as:

$$c^2 = kRT \quad (5)$$

where R is the gas constant, k is the ratio between the specific heat at constant pressure and volume, and T is the medium temperature. To the purpose of this study, a constant temperature and homogeneous chemical composition was imposed, hence c has a known and constant value. The assumed value of T is in agreement with [4] and with the typical EGR exhaust gas temperatures; on the other hand, to assess the method operation an arbitrary value could be used.

For the sake of simplicity, air was used as a medium (and was considered as a homogeneous gas with $k = 1.4$). Moreover, only axial flow was considered, thus the angle α becomes known from the problem geometry (i.e., from the ERCs positioning). In these conditions, the model stated in Eq. 4 becomes linear.

To estimate the velocity field U , the domain on the plane Ω was divided into several rectangular mesh according to the scheme showed in Fig.2, where a single cell element is highlighted.

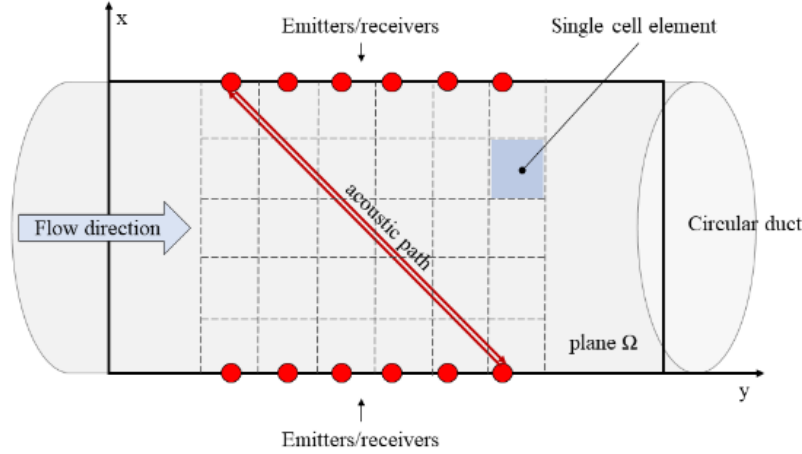


Figure 2. Measurement setup scheme.

Emitter-receiver couples are placed in a known position at domain boundaries, parallel to flow direction, on plane Ω . The j -th acoustic path cross only some mesh element (i), thus the path l_j can be described as the sum of all the sub-paths Δl_{ji} . Therefore, Eq. 4 can be discretized as follows:

$$\frac{\Delta \tau_j}{2} = \frac{1}{c^2} \sum_i U_i \cos(\alpha_j) \Delta l_{ji} \quad (6)$$

The terms U_i indicates the average axial flow speed in the i -th cell element. Therefore, by measuring $\Delta \tau_j$ for each path, the linear system in Eq.6 can be solved and the velocity field calculated. It must be ensured that, in a single cell, at least one path is present, and that the equation number is greater or equal to the number of cells. Similar procedure is used in [5] to reconstruct the temperature field with acoustic pyrometry method. Generally, Eq.6 describes an overdetermined linear system, and several methods can be used to calculate the solution [2,6,7]. In this work, a Matlab routine based on the least square minimization of the residual norm was used with satisfactory results. In particular, the algorithm search for the vector of U_i that minimizes the following:

$$\sum_j \frac{\Delta \tau_j}{2} - \frac{1}{c^2} \sum_i U_i \cos(\alpha_j) \Delta l_{ji} \quad (7)$$

As a benchmark profile U^* , a gaussian-shaped velocity was considered over the y -axis, and exponentially decaying along the x -axis as showed in Fig. 3. The profile is then described by Eq. 8:

$$U^*(x, y) = U_{max} e^{-\frac{(x-\mu)^2}{2\sigma^2}} e^{-\frac{y}{2}} \quad (8)$$

Where μ , σ and U_{max} are chosen, respectively, as 0.5 m, 0.4 m and 100 m/s.

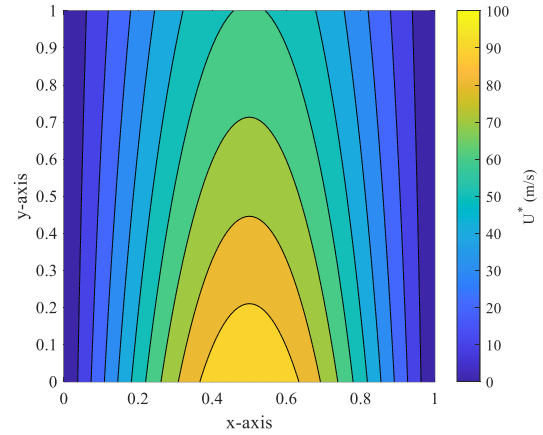


Figure 3. Velocity profile used as case study

Starting from the benchmark profile U^* , the $\Delta \tau_j$ values can be simulated as a function of the ERCs positioning. Indeed, by knowing the problem geometry i.e., the α_j , and the path connecting the ERCs, the line integral in Eq. 4 can be calculated, thus the j -th $\Delta \tau_j$ can be obtained. Therefore, the velocity U_i can be reconstructed according to Eq.7 as a function of the ERCs number N_{ERC} , and of the used computational domain in terms of its distribution and element number N_{mesh} . An example of the used computational domain is showed in Fig. 4.

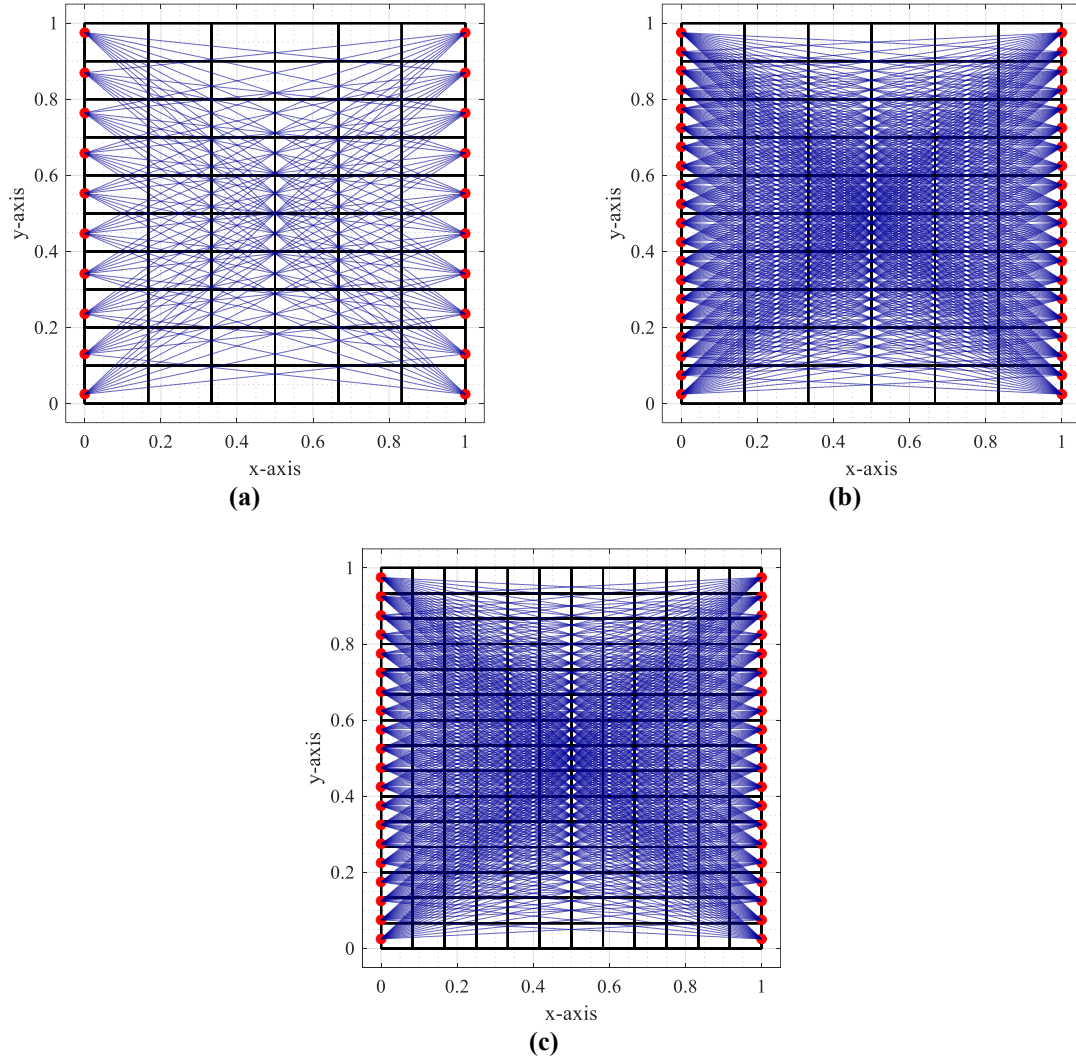


Figure 4. Typical domains used in the case study: 60 cells and 10 ERCs per side (a), 60 cells and 20 ERCs per side (b), and 195 cells and 20 ERCs per side (c). The red dots represent the ERCs, the black lines the mesh distribution, and the blue lines the considered sound paths.

In comparison to the temperature estimation by acoustic pyrometry methods [8], the reconstruction significantly depends on the angle between the acoustic path and the flow velocity direction angle, and hence requires a more complex approach. Moreover, particular attention should be paid to the path with α_j close to 90° , for which the terms $\cos(\alpha_j)$ tend to zero. In the configuration shown in Fig. 4, this condition could be possibly achieved at the bottom and at the top of the y-axis position. This might result in a bad conditioned problem. The study of this problem is out of the scope of this study.

For a given number of ERCs the reconstructed field is expected to improve as N_{mesh} increases until at least one path is present in each cell. Therefore, the reconstruction capability of the model is investigated by comparing the best reconstruction of U^* , given N_{mesh} , with the reconstructed field U . The

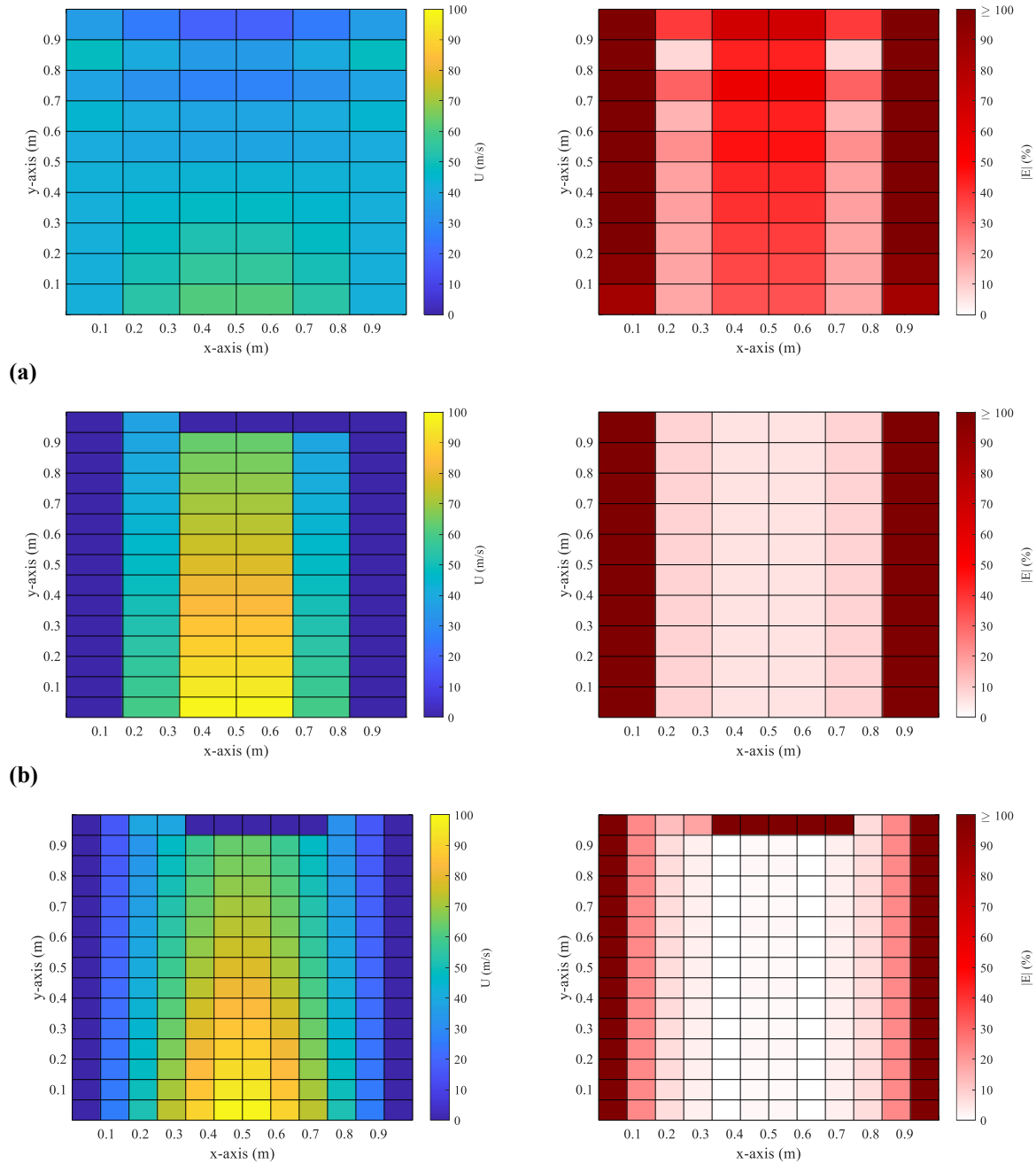
best reconstruction of U^* , $U_{best}^*(N_{mesh})$, is calculated by averaging U^* on each single cell element, thus the index E is calculated as:

$$E = 1 - \frac{U}{U_{best}^*(N_{mesh})} \quad (9)$$

Finally, the average, maximum and minimum values of E are considered for comparison purposes.

RESULTS AND DISCUSSION

The contour map reporting the reconstructed velocity field U and the error map E for three significant cases is showed in Fig. 5.



(a) **Figure 5. Reconstructed velocity field U (left figures) and error map E (right figures) for different configurations: 60 cells and 15 ERCs per side (a), 60 cells and 20 ERCs per side (b), and 180 cells and 20 ERCs per side (c).**

In all the cases, the residual calculation for the problem in Eq. 4 is below 10^{-18} s. For the case presented in Fig. 5, the cells on the domain side are critical, showing very large errors i.e., above 100%. Indeed, according to Eq. 8, as U^* approaches to 0, the absolute value of E increases indefinitely. Large errors are found at the top and at the bottom of y -axis, where many acoustic paths are nearly orthogonal to the axial velocity U (see Fig. 5b and 5c). On the other hand, for the cases in Fig. 5b and

5c, the error in the center of the domain is contained within 10%.

Fig. 6 shows the behavior of the average of E as a function of the cells number for the case of 20 ERCs per side.

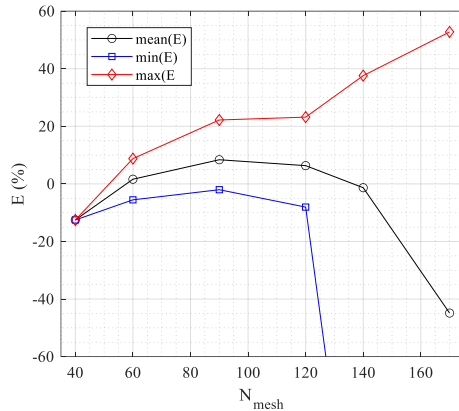


Figure 6. Behavior of the average of E as a function of the cells number for the case of 20 ERCs per side.

Fig. 6 shows that for a low mesh number, the minimum, maximum and average errors collapse. This occurs due to large cells elements, which promote a uniform velocity field as solution of the system in Eq.6 (see e.g., Fig. 5a). By increasing the number of mesh elements, the amount of path per cell decreases, and the number of cells with $\cos(\alpha_j)$ close to zero increases, as shown by comparing Fig. 4b and 4c. Indeed, as shown in Fig. 5, the main error entity is distributed on domain boundary.

Results show that the axial velocity field reconstruction is possible. Nonetheless, the solution is sensitive to the analysis parameters, such as the cells number, their distribution, and the ERCs number. In addition, the dependence is complex and, generally, not straightforward to predict. Further analysis to study the effect of the specific solution strategy on the result, and the impact of different boundary conditions should be studied to enhance the reliability of the presented method.

CONCLUSIONS

The 2D reconstruction of the velocity field is performed by an acoustic tomography method on simulated test case. A series of acoustic emitters and receivers are used to evaluate the time of flight of an acoustic wave. This is mainly influenced by the problem geometry, usually known, and by the flow speed distribution. A purposely developed model was used to reconstruct the velocity profile by this information. As first, a benchmark velocity profile is considered to simulate the measurement of the time of flight. Therefore, the obtained velocity field was assessed as a function of the number of ERCs and the domain grid employed in the reconstruction algorithm. From the results, the velocity field was calculated within 10% error against the benchmark profile, especially in the central domain region. On the other hand, side areas of the domain along the y -axis might be affected by numerical error due to the

calculation of very small angles, given by the problem geometry. As a preliminary result, it was shown that the chosen domain and ERCs positioning optimization has a crucial role for a reliable reconstruction field, and that the value of E as a function of these parameters is not straightforward to predict.

REFERENCES

- [1] M. Starke, A. Raabe, Acoustic tomographic imaging of temperature and flow fields in air, *Meas. Sci. Technol.* 22 (2011).
- [2] A. Ziemann, K. Arnold, A. Raabe, Acoustic tomography in the atmospheric surface layer, *Ann. Geophys.* 17 (1998).
- [3] Y.-Q. Li, H.-C. Zhou, Experimental study on acoustic vector tomography of 2-D flow field in an experiment-scale furnace, *Flow Meas. Instrum.* 17 (2006).
- [4] U. Desilva, R. Bunce, H. Claussen, Novel Gas Turbine Exhaust Temperature Measurement System, *Proceedings of the ASME Turbo Expo* (2013).
- [5] G. Caposciutti, L. Ferrari, Acoustic Pyrometry Robustness To Time Of Flight Estimation Errors, *J. Eng. Gas Turbines Power.* 144 (2021).
- [6] S.K. Chaitanya, J.K.K. Alapati, K. Srinivasan, Evaluation of regularization methods for acoustic pyrometry, *Measurement.* 198 (2022). [https://doi.org/https://doi.org/10.1016/j.measurement.\(2022\)](https://doi.org/https://doi.org/10.1016/j.measurement.(2022)).
- [7] Y. Li, Y. Wang, X. Guan, H. Zhou, X. Ma, A wavelet model on reconstructing complex aerodynamic field in furnace with acoustic tomography, *Measurement.* 157 (2020).
- [8] L. Ferrari; G. Caposciutti; G. Pasini; G. F. Frate; U. Desideri, Influence Of Emitter-Receiver Number On Measurement Accuracy In Acoustic Pyrometry, in: *E3S Web Conf.* Vol. 345, 2022. XXV Bienn. Symp. Meas. Tech. Turbomach. MTT 2020 (2022).